

Diffraction of atomic matter waves through a 2D crystal

Carina Kanitz¹, Jakob Bühler¹, Vladimír Zobač², Joseph J. Robinson¹, Toma Susi^{2†},
Maxime Debiossac¹, and Christian Brand^{1,*}

¹German Aerospace Center (DLR), Institute of Quantum Technologies, Wilhelm-Runge-
Strasse 10, 89081 Ulm, Germany

²University of Vienna, Faculty of Physics, Boltzmannngasse 5, 1090 Vienna, Austria

† E-mail: Toma.Susi@univie.ac.at

* E-mail: Christian.Brand@dlr.de

Interferometry of atomic matter waves is an essential tool in fundamental sciences¹⁻⁵ and for applied quantum sensors⁶⁻¹⁰. The sensitivity of interferometers scales with the momentum separation of the diffracted matter waves, leading to the development of large-momentum transfer beam splitters^{11,12}. However, despite decades of research, crystalline gratings used since the first atomic diffraction experiments are still unmatched regarding momentum transfer¹³. So far, diffraction through such gratings has only been reported for subatomic particles, but never for atoms. Here, we answer to this century-old challenge by demonstrating diffraction of helium and hydrogen atoms at kiloelectronvolt energies through single-layer graphene at normal incidence. Despite the atoms' high kinetic energy and coupling to the electronic system of graphene, we observe diffraction patterns featuring coherent scattering of up to eight reciprocal lattice vectors. Diffraction in this regime is possible due to the short interaction time of the projectile with the atomically-thin crystal, limiting the momentum transfer to the grating. Our demonstration is the atomic counterpart of the first transmission experiments with electrons by Thomson and Reid^{14,15}, unlocking new potentials in atom diffraction. We expect our findings to inspire studies of decoherence in an uncharted energy regime and the development of new matter-wave-based sensors.

A mere seven years after Louis de Broglie published his seminal work on the wave nature of massive particles in 1923¹⁶, diffraction had been demonstrated for electrons^{14,17}, atoms, and diatomic molecules¹³. Key to this success were crystalline materials that act as gratings for matter waves. They were used in reflection for electrons by Davisson and Germer¹⁷, and for atoms and molecules by Estermann and Stern¹³. Crystal lattices also played a critical role in demonstrating diffraction of electrons in transmission by Thomson¹⁵.

While electron diffraction revolutionised microscopy¹⁸, atom interferometry became an indispensable tool for modern physics due to the atoms' susceptibility to a wide variety of forces and fields^{1,19}. Nowadays, atom interferometers are used to measure atomic properties^{20,21}, define fundamental constants^{2,22-24}, and search for new physics beyond the standard model^{25,26}.

The sensitivity of all interferometers scales with the momentum imparted by the grating to the matter wave. Hence, it is advantageous to use large-momentum transfer beam splitters^{23,27,28}, corresponding to small grating periods. Laser-based gratings in combination with accelerated optical lattices (Bloch oscillations) can transfer up to a thousand photon momenta²². Although nearly arbitrary patterns can be etched into nanomechanical membranes²⁹⁻³¹, their grating period is currently limited to about 100 nm by the machining process^{32,33}. Thus, even after decades of research, the momentum transfer imparted by crystals remains unmatched.

So far, atomic diffraction using crystalline materials has always been studied in reflection³⁴⁻³⁶. This raises the fundamental question of whether it is possible to demonstrate atomic diffraction also through a crystal. To achieve this feat, the coherence of the matter wave has to be preserved during transmission. This requires that the interaction between atom and crystal is sufficiently weak to obscure the exact path of the projectile through the grating. During the passage, the distance between the matter wave and the grating atoms is on the order of an Ångström, leading to a significant overlap of the atomic orbitals of the projectile with those of the grating. Transmitting the atom through the crystal while preserving coherence therefore seems a formidable task.

We answer to this century-old challenge by demonstrating diffraction of helium and atomic hydrogen through free-standing single-layer graphene. This diffraction through a crystalline material is the atomic counterpart of the experiment by Thomson¹⁵. Graphene has a grating period of 246 pm, 400 times smaller than state-of-the-art nano-machined transmission masks and more than 3,000 times smaller than the wavelength used to manipulate rubidium atoms. Thus, our experiment realises the beamsplitter with the currently largest momentum transfer for atoms in transmission.

We use atoms with a kinetic energy E normal to the lattice of up to 1.6 keV, three orders of magnitude larger than in any previous atomic diffraction experiment^{34,36,37}. Diffraction in this regime is even more surprising as the atoms should have sufficient energy to damage the crystalline grating³⁸. We thus explore a completely uncharted interaction regime, fundamentally different from any previous atomic diffraction experiment.

Atom-Crystal interaction

Due to its outstanding electronic and mechanical properties, single-layer graphene is the perfect candidate to act as a grating for atoms in transmission. Further, it can be routinely prepared as free-standing material on suitable support structures. Regarding the matter wave, helium is a reasonable choice as it is inert and the smallest neutral atom. Although atomic hydrogen is lighter than helium, its unpaired electron leads to stronger couplings to graphene^{39,40}, which might destroy the coherence of the matter wave.

To find suitable experimental conditions for diffraction, we model the interaction of the atoms with the crystal using time-dependent density functional theory molecular dynamics simulations, see Fig. 1. The most critical parameters are the energy loss to the grating and the exchanged transverse momentum Δp ⁴¹. As long as Δp is below Heisenberg's momentum uncertainty p_0 of the carbon atoms in graphene, coherence should be preserved. The momentum uncertainty can be estimated as $m_C \sqrt{\langle v^2 \rangle} = 2.1 \times 10^{-23}$ kg m/s with $\langle v^2 \rangle$ the mean-square in-plane velocity and m_C the mass of the carbon atom⁴¹. For helium transmitted through the centre of a hexagon, the simulations predict that Δp is smaller than p_0 for a beam energy E above 100 eV, as shown in Fig. 1(b).

This by itself may appear counter-intuitive. At ambient conditions, helium does not penetrate single-layer graphene⁴². Thus, we have to increase the atom's energy to push it through the grating. However, this does not lead to an increased momentum transfer because the interaction time is decreasing, see Fig. 1(a). By making the atoms faster, we can also mitigate the increase of Δp when the projectile passes the crystal closer to a grating atom⁴¹.

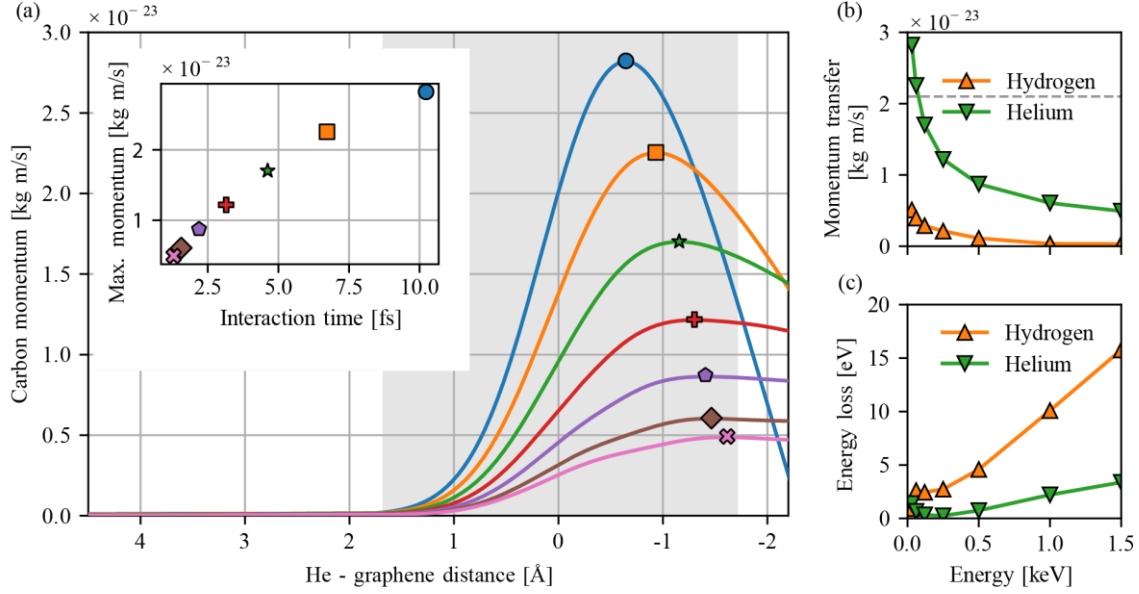


Figure 1 | Coupling of fast atoms to graphene. (a) Momentum of a carbon atom during the interaction with helium at different kinetic energies: 30 eV (circle), 60 eV (square), 120 eV (star), 250 eV (plus), 500 eV (pentagon), 1000 eV (diamond), and 1500 eV (cross). The grey area shows the van der Waals interaction region of ± 1.7 Å. The inset shows the corresponding interaction time (duration for the projectile passing through the interaction region). (b) Transverse momentum transfer to a carbon atom while He or H pass the material depending on the projectile kinetic energy. The broken line corresponds to the in-plane momentum uncertainty of C in graphene. (c) Energy loss to the electronic system while He or H pass the material depending on the projectile kinetic energy. In (b-c) the symbols are calculations and the lines are to guide the eye.

A higher beam energy, however, also enhances the energy loss to the electronic structure of graphene, see Fig. 1(c). The energy loss has a minimum around $E = 250$ eV, increases with beam energy, and reaches several electronvolts at $E = 1500$ eV. A good compromise between the energy loss and the momentum transfer is expected for beam energies between 400 and 600 eV.

For hydrogen, the momentum transfer to the crystalline lattice is smaller by about an order of magnitude compared to helium, cf. Fig. 1(b). At the same time, the energy loss to graphene is much more pronounced, reaching 16 eV at a beam energy of 1.5 keV.

Diffraction of atoms through a 2D crystal

A schematic of the experimental setup is depicted in Fig. 2(a) and described in more detail in the Methods. We prepare a beam of helium ions or protons in the energy range between 390 and 1600 eV with an ion gun and then neutralise it using a gas-filled charge-exchange cell^{37,43}. The de Broglie wavelength $\lambda_{dB} = h/\sqrt{2mE}$ of the atoms is defined by the beam kinetic energy E , the atomic mass m , and Planck's constant h . In the considered energy range, λ_{dB} lies between 400 and 950 fm. At the position of the grating, the transverse coherence amounts to a least five times the lattice constant a of graphene and the minimum longitudinal coherence is about $50 \times \lambda_{dB}$. This is sufficient for multi-slit diffraction.

The matter wave impinges with a momentum $\hbar k = h/\lambda_{dB}$ at the honeycomb lattice of graphene, with reduced Planck constant \hbar . During diffraction, the grating imparts transverse momentum to the matter wave in integer multiples of the reciprocal basis vectors $\hbar \mathbf{G}_1$ and $\hbar \mathbf{G}_2$.

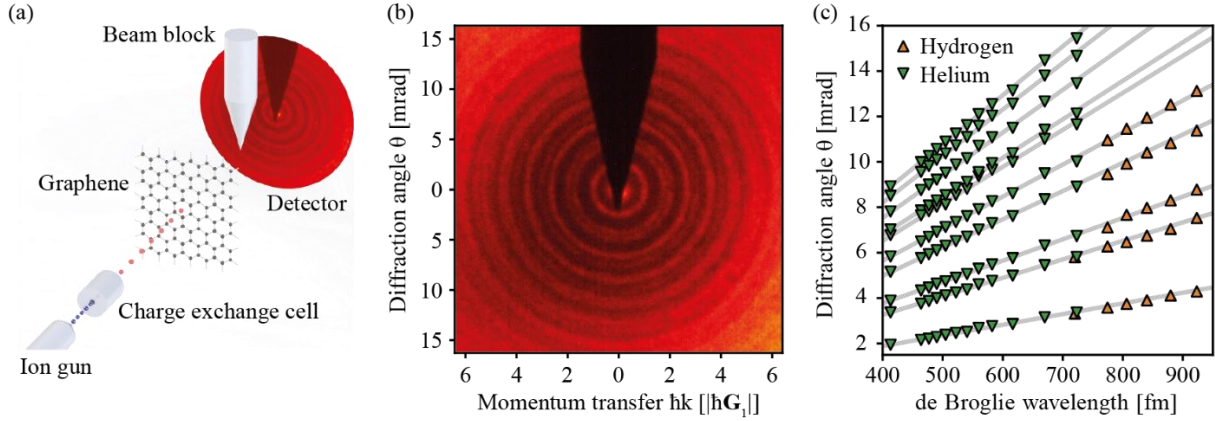


Figure 2 | Atomic diffraction through polycrystalline free-standing single-layer graphene. (a) A beam of H^+ or He^+ (blue spheres) is prepared using an ion gun and then neutralised in a charge-exchange cell. After collimation to 1 mrad (FWHM) the neutral beam (red spheres) impinges onto the graphene sample at normal incidence. The transmitted signal is visualised using a position-sensitive detector (microchannel plate) stacked onto a phosphorous screen and recorded with a CMOS camera. (b) Diffraction of helium at 706 eV through polycrystalline graphene results in Debye-Scherrer rings exhibiting diffraction angles of more than 15 mrad. (c) Experimental verification of the diffraction equation. The diffraction angle θ of H (yellow) and He (green) is plotted versus the de Broglie wavelength (corresponding to kinetic energies between 390 and 1600 eV). The lines represent expected diffraction angles $\sin(\theta) = |\mathbf{G}|/k$.

Those are proportional to the inverse of the lattice constant a , see Methods. The diffraction angle θ is then given by the ratio of imparted momentum to forward momentum $\sin(\theta) = |\mathbf{G}|/k$, where $\mathbf{G} = n_1\mathbf{G}_1 + n_2\mathbf{G}_2$. The small lattice constant leads to diffraction angles on the order of several milliradians that can be well resolved with a position-sensitive detector, see Fig. 2.

In our experiment, the atomic beam has a diameter of about 300 μm when it reaches the polycrystalline suspended graphene. Instead of individual diffraction peaks arising from a single lattice orientation, we thus expect Debye-Scherrer rings⁴⁴, reflecting the random orientations of the different crystal domains in the sample. We are able to resolve patterns exhibiting more than 10 distinct rings at angles reaching up to 15 mrad, as shown in Fig. 2(b). To verify whether the peaks are due to diffraction, we plot the angular positions of the Debye-Scherrer rings against the de Broglie wavelength. As shown in Fig. 2(c), we observe an excellent agreement between the experimental data and the theoretical diffraction angles both for H and He. We therefore conclude that the patterns result from the coherent interaction with the lattice and are due to diffraction.

Damping of diffraction orders

Whereas the beam energy determines the peak positions, simulations predict that it also influences the couplings to the crystal. To explore this, we compare the azimuthally averaged intensity traces for helium at various beam energies, as shown in Fig. 3(a). At the lowest energy, we can distinguish more than 20 diffraction rings. They correspond to about eight reciprocal vectors exchanged with the surface, as \mathbf{G}_1 and \mathbf{G}_2 span a 2D lattice, see Methods.

With increasing energy, the higher diffraction orders vanish and are replaced by a broad unstructured background. This becomes dominant at large diffraction angles, that is, when $k > 8 \cdot |\mathbf{G}_1|$ at $E = 1208$ eV. That trend persists even when increasing the angular resolution of the experiment, see Methods.

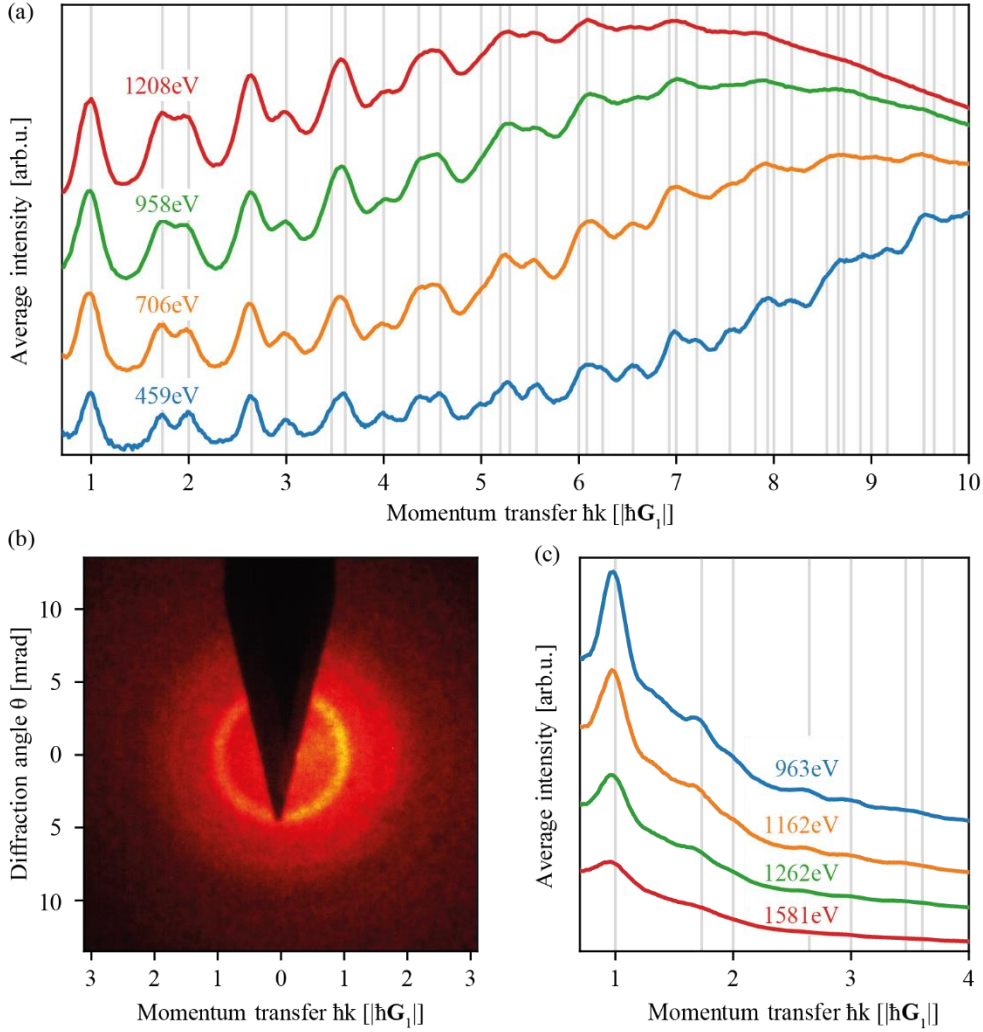


Figure 3 | **Energy-dependent atomic diffraction through single-layer graphene.** The experimental azimuthally averaged intensity at various kinetic energies is plotted versus momentum transfer in units of the graphene reciprocal lattice vector \mathbf{G}_1 for He (a) and H (c). Vertical lines indicate the calculated diffraction angles. (b) Diffraction pattern of H atoms at 963 eV.

For hydrogen, the damping of higher diffraction orders is even more pronounced and the patterns consist only of a few diffraction orders, as shown in Fig. 3(b, c). Nevertheless, we observe diffraction for hydrogen in the energy range from 1.0 to 1.6 keV. These observations are fascinating, as they suggest that the atoms have lost several electronvolts of energy to the grating yet still preserve coherence.

Discussion and Outlook

We have demonstrated the first diffraction of atomic matter waves through a crystalline material. This realises the atomic counterpart of the experiment conducted by Thomson with electrons¹⁵, responding to a century-old challenge. Although we expect significant couplings to the grating, we are able to resolve diffraction patterns corresponding to momentum transfers of up to $\pm 8 \hbar|\mathbf{G}_1|$. Comparing to existing beam splitting techniques in atom interferometry, for instance with Rb atoms, scattering more than 50,000 photons at 780 nm would be necessary to impart the same momentum splitting. Our platform thus realises the beamsplitter with the largest known momentum transfer for atoms in transmission.

To achieve this, we illuminated graphene at normal incidence with atomic beams in the kiloelectronvolt energy range. Although some samples were irradiated for more than 100 hours, we did not observe any degradation of the grating's performance. Thus, our demonstration opens the door towards studying diffraction in an uncharted regime of interaction energies. We expect this to be a rich field to study decoherence both experimentally and theoretically. Especially the use of single crystals is interesting as it would allow for separating coherent and incoherent contributions of the diffraction patterns. Further, it would be fascinating to extend the experiments to other crystals and a larger range of energies.

Combining crystalline transmission gratings into interferometers might give rise to new quantum-based sensors. Fast atoms have advantages for detecting gravitational waves^{45,46} compared to cold-atom experiments^{47,48} and might give rise to new multi-dimensional interferometers⁴⁹.

References

- 1 Cronin, A. D., Schmiedmayer, J. & Pritchard, D. E. Optics and interferometry with atoms and molecules. *Rev. Mod. Phys.* **81**, 1051-1129 (2009).
- 2 Parker, R. H., Yu, C., Zhong, W., Estey, B. & Müller, H. Measurement of the fine-structure constant as a test of the Standard Model. *Science* **360**, 191 (2018).
- 3 Rosi, G., Sorrentino, F., Cacciapuoti, L., Prevedelli, M. & Tino, G. M. Precision measurement of the Newtonian gravitational constant using cold atoms. *Nature* **510**, 518-521 (2014).
- 4 Asenbaum, P., Overstreet, C., Kim, M., Curti, J. & Kasevich, M. A. Atom-Interferometric Test of the Equivalence Principle at the 10^{-12} Level. *Phys. Rev. Lett.* **125**, 191101 (2020).
- 5 Becker, D. *et al.* Space-borne Bose–Einstein condensation for precision interferometry. *Nature* **562**, 391-395 (2018).
- 6 Bongs, K. *et al.* Taking atom interferometric quantum sensors from the laboratory to real-world applications. *Nat. Rev. Phys.* **1**, 731-739 (2019).
- 7 Barrett, B. *et al.* Dual matter-wave inertial sensors in weightlessness. *Nat. Commun.* **7**, 13786 (2016).
- 8 Wu, X. *et al.* Gravity surveys using a mobile atom interferometer. *Sci. Adv.* **5**, eaax0800 (2019).
- 9 Amico, L. *et al.* Colloquium: Atomtronic circuits: From many-body physics to quantum technologies. *Rev. Mod. Phys.* **94**, 041001 (2022).
- 10 Schleich, W. P. *et al.* Quantum technology: from research to application. *Appl. Phys. B* **122**, 130 (2016).
- 11 Chiow, S.-w., Kovachy, T., Chien, H.-C. & Kasevich, M. A. $102 \hbar k$ Large Area Atom Interferometers. *Phys. Rev. Lett.* **107**, 130403 (2011).
- 12 Müller, H., Chiow, S.-w., Long, Q., Herrmann, S. & Chu, S. Atom Interferometry with up to 24-Photon-Momentum-Transfer Beam Splitters. *Phys. Rev. Lett.* **100**, 180405 (2008).
- 13 Estermann, I. & Stern, O. Beugung von Molekularstrahlen. *Z. Phys.* **61**, 95-125 (1930).
- 14 Thomson, G. P. & Reid, A. Diffraction of Cathode Rays by a Thin Film. *Nature* **119**, 890-890 (1927).
- 15 Thomson, G. P. The diffraction of cathode rays by thin films of platinum. *Nature* **120**, 802-802 (1927).
- 16 Broglie, L. d. Waves and Quanta. *Nature* **112**, 540 (1923).
- 17 Davisson, C. & Germer, L. H. The scattering of electrons by a single crystal of Nickel. *Nature* **119**, 558-560 (1927).
- 18 Ruska, E. The development of the electron microscope and of electron microscopy. *Rev. Mod. Phys.* **59**, 627-638 (1987).
- 19 Berman, P. R. *Atom Interferometry*. (Academic Press, 1997).

- 20 Holmgren, W. F., Reville, M. C., Lonij, V. P. A. & Cronin, A. D. Absolute and ratio measurements of the polarizability of Na, K, and Rb with an atom interferometer. *Phys. Rev. A* **81**, 053607 (2010).
- 21 Fein, Y. Y. *et al.* Quantum-Assisted Measurement of Atomic Diamagnetism. *Phys. Rev. X* **10**, 011014 (2020).
- 22 Morel, L., Yao, Z., Cladé, P. & Guellati-Khélifa, S. Determination of the fine-structure constant with an accuracy of 81 parts per trillion. *Nature* **588**, 61-65 (2020).
- 23 Panda, C. D. *et al.* Coherence limits in lattice atom interferometry at the one-minute scale. *Nat. Phys.* **20**, 1234-1239 (2024).
- 24 Fixler, J. B., Foster, G. T., McGuirk, J. M. & Kasevich, M. A. Atom interferometer measurement of the Newtonian constant of gravity. *Science* **315**, 74-77 (2007).
- 25 Hamilton, P. *et al.* Atom-interferometry constraints on dark energy. *Science* **349**, 849-851 (2015).
- 26 Safronova, M. S. *et al.* Search for new physics with atoms and molecules. *Rev. Mod. Phys.* **90**, 025008 (2018).
- 27 Kovachy, T. *et al.* Quantum superposition at the half-metre scale. *Nature* **528**, 530-533 (2015).
- 28 Gebbe, M. *et al.* Twin-lattice atom interferometry. *Nat. Commun.* **12**, 2544 (2021).
- 29 Keith, D. W., Schattenburg, M. L., Smith, H. I. & Pritchard, D. E. Diffraction of Atoms by a Transmission Grating. *Phys. Rev. Lett.* **61**, 1580-1583 (1988).
- 30 Carnal, O., Sigel, M., Sleator, T., Takuma, H. & Mlynek, J. Imaging and focusing of atoms by a Fresnel zone plate. *Phys. Rev. Lett.* **67**, 3231-3234 (1991).
- 31 Fujita, J. *et al.* Manipulation of an atomic beam by a computer-generated hologram. *Nature* **380**, 691-694 (1996).
- 32 Savas, T. A., Shah, S. N., Schattenburg, M. L., Carter, J. M. & Smith, H. I. Achromatic interferometric lithography for 100-nm-period gratings and grids. *J. Vac. Sci.; Technol. B* **13**, 2732-2735 (1995).
- 33 Juffmann, T. *et al.* Real-time single-molecule imaging of quantum interference. *Nat. Nanotechnol.* **7**, 297-300 (2012).
- 34 Jardine, A. P. *et al.* Ultrahigh-Resolution Spin-Echo Measurement of Surface Potential Energy Landscapes. *Science* **304**, 1790-1793 (2004).
- 35 Winter, H. & Schüller, A. Fast atom diffraction during grazing scattering from surfaces. *Prog. Surf. Sci.* **86**, 169-221 (2011).
- 36 Farias, D. & Rieder, K.-H. Atomic beam diffraction from solid surfaces. *Rep. Prog. Phys.* **61**, 1575 (1998).
- 37 Rousseau, P., Khemliche, H., Borisov, A. G. & Roncin, P. Quantum Scattering of Fast Atoms and Molecules on Surfaces. *Phys. Rev. Lett.* **98**, 016104 (2007).
- 38 Lehtinen, O. *et al.* Effects of ion bombardment on a two-dimensional target: Atomistic simulations of graphene irradiation. *Phys. Rev. B* **81**, 153401 (2010).
- 39 Lienemann, J. *et al.* Coherence during scattering of fast H atoms from a LiF(001) surface. *Phys. Rev. Lett.* **106**, 067602 (2011).
- 40 Jiang, H. *et al.* Imaging covalent bond formation by H atom scattering from graphene. *Science* **364**, 379 (2019).
- 41 Brand, C. *et al.* Coherent diffraction of hydrogen through the 246 pm lattice of graphene. *New J. Phys.* **21**, 033004 (2019).
- 42 Bunch, J. S. *et al.* Impermeable Atomic Membranes from Graphene Sheets. *Nano Lett.* **8**, 2458-2462 (2008).
- 43 Schüller, A., Wethekam, S. & Winter, H. Diffraction of fast atomic projectiles during grazing scattering from a LiF(001) surface. *Phys. Rev. Lett.* **98**, 016103 (2007).
- 44 Pecharsky, V. K. & Zavalij, P. Y. *Fundamentals of Powder Diffraction and Structural Characterization of Materials*. 2 edn, (Springer New York, 2009).

- 45 Chiao, R. Y. & Speliotopoulos, A. D. Towards MIGO, the matter-wave interferometric gravitational-wave observatory, and the intersection of quantum mechanics with general relativity. *J. Mod. Opt.* **51**, 861-899 (2004).
- 46 Graham, P. W., Hogan, J. M., Kasevich, M. A. & Rajendran, S. New method for gravitational wave detection with atomic sensors. *Phys. Rev. Lett.* **110**, 171102 (2013).
- 47 Lamine, B., Hervé, R., Lambrecht, A. & Reynaud, S. Ultimate decoherence border for matter-wave interferometry. *Phys. Rev. Lett.* **96**, 050405 (2006).
- 48 Roura, A., Brill, D. R., Hu, B. L., Misner, C. W. & Phillips, W. D. Gravitational wave detectors based on matter wave interferometers (MIGO) are no better than laser interferometers (LIGO). *Phys. Rev. D* **73**, 084018 (2006).
- 49 Barrett, B., Cheiney, P., Battelier, B., Napolitano, F. & Bouyer, P. Multidimensional Atom Optics and Interferometry. *Phys. Rev. Lett.* **122**, 043604 (2019).

Methods

Experimental Setup

We create a beam of protons or helium ions using a commercial ion gun including a Wien filter (Nonsequitur Technologies model 1402W). The resulting beam energy E and its energy distribution ΔE are measured using a retractable Faraday cup (Kimball Physics FC-71) equipped with a retarding grid. Typical full width at half maximum values obtained for ΔE are 24 eV for H^+ and 18 eV for He^+ . To neutralise the beam, the ions are guided into a 38 mm long charge-exchange cell filled with a neutral gas. We use He as neutralisation gas for He^+ and Ar in the case of the protons. The pressure inside the cell is optimised for neutral beam intensity as well as beam convergence, and is typically in the range of 5×10^{-2} mbar. We note that neutralisation of H^+ on Ar leads to an energy loss of 2.6 eV⁵⁰. However, this is too little to be observable in the experiment.

The entrance and exit of the charge-exchange cell are closed off by two pinholes that can be varied in diameter. Unless stated otherwise, the pinholes at the entrance and exit have a diameter of $s_0 = 1$ mm and $s_1 = 500$ μm respectively. Remaining ions behind the charge-exchange cell are removed from the beam with a deflection voltage. The neutral beam is collimated by a $s_2 = 200$ μm wide pinhole situated at $L = 790$ mm behind the charge-exchange cell, resulting in a collimation angle of $\varphi = (s_1 + s_2)/L \approx 1$ mrad.

As gratings, we use commercially available monolayer graphene suspended over a holey silicon nitride substrate (Plano GmbH 21712). Individual holes in the substrate have a diameter of 2.5 μm and cover an area of 500×500 μm^2 . These samples are positioned into the beam using a five-axis manipulator. The transverse coherence ℓ_t of the matter wave at the position of the grating can be estimated as $\ell_t = 2L\lambda_{dB}/s_1$ ⁵¹, resulting in $\ell_t \geq 5a$. The longitudinal coherence ℓ_l is given by $\lambda_{dB}^2/\Delta\lambda_{dB} \geq 50\lambda_{dB}$.

After diffraction, the atoms propagate 727 mm until they impinge on a double-stack microchannel detector stacked onto a phosphorous screen. The detector has an active diameter of 75 mm and a pore size of 10 μm . The pattern is recorded using a CMOS camera (Hamamatsu Orca Flash 4.0) equipped with a zoom objective (Computar TEC-V7X). To reduce the background, we use a bandpass filter transmitting in the wavelength range between 535 and 558 nm (Midopt BI550) optimised for the peak emission of the phosphor P43 at 545 nm. The direct beam is blocked from reaching the detector using a metal thorn on a linear drive.

Before the start of the experiment, the graphene samples are annealed in vacuum at 450°C for 90 min⁵². Additionally, we clean the sample in high vacuum by illuminating it with a 300 mW cw laser emitting at 532 nm. This procedure provides sufficiently clean samples⁵³ to observe diffraction patterns. When diffracting H atoms through graphene, the grating was illuminated with the cleaning laser every 60 minutes to remove adsorbed atoms. In the case of helium diffraction, it was sufficient to laser-clean the sample once per day.

Image correction and post-processing

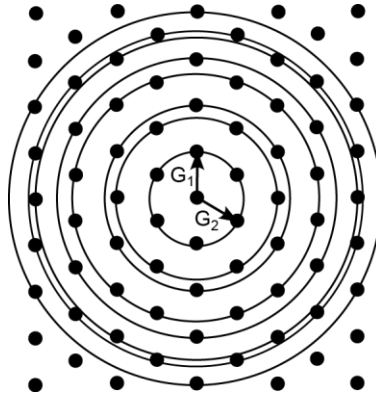
Images were recorded in series. Each element of a series corresponds to 300 images with an exposure time of 1 s, which were integrated into one image. In total, we acquired data for one to four hours to arrive at the traces shown in Fig. 3 of the main manuscript. For the data needed to confirm the diffraction angles with varying energy in Fig. 2(c), an acquisition time of 15 minutes was sufficient. All recorded images were compensated for radial objective distortion

up to the quadratic term. Due to the software used, the intensity values needed to be rescaled before they could be combined or compared. Rescaling was performed to a region of known brightness common to all images outside of the detector area. Camera dark count correction was performed with the camera cap on with a 5-minute integration time.

After corrections, all recorded images from a measurement series were averaged together into a single image and cropped around the region of interest. To determine the centre of the pattern, the inner diffraction rings were fit with a 2D-function by modelling rings as Gaussian in the radial direction and as uniform along the azimuthal angle. For generating radial traces, the area of the screen covered by the beam block was excluded.

Debye-Scherrer rings

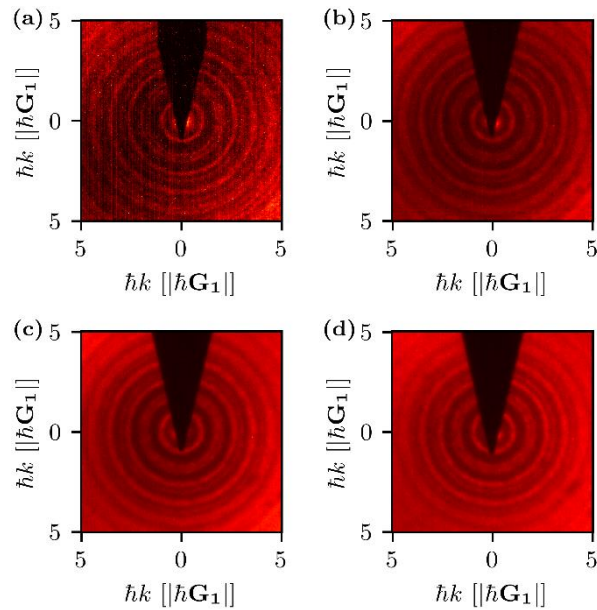
The radii of the Debye-Scherrer rings follow the expected positions according to the diffraction equation. The magnitude of both reciprocal basis vectors \mathbf{G}_1 and \mathbf{G}_2 is $4\pi/(\sqrt{3}a)$ with $a = 246$ nm the lattice constant of graphene. We can visualise the positions of the rings in reciprocal space, as shown in Extended Data Fig. 1. Here, the black spots represent the locations of the diffraction spots for a single crystal. The circles are the Debye-Scherrer rings resulting from azimuthally rotating each set of spots around the origin, which originate from the polycrystalline nature of the graphene samples used.



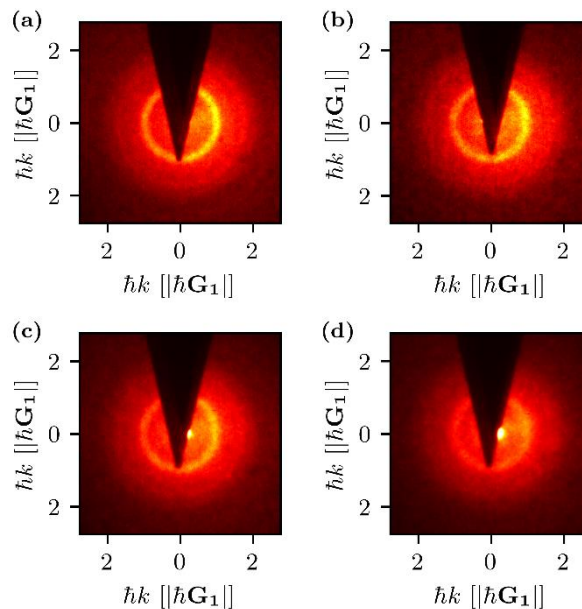
Extended Data Figure 1 | Debye-Scherrer rings corresponding to the diffraction spots for monolayer graphene. The vectors \mathbf{G}_1 and \mathbf{G}_2 are the reciprocal vectors of the lattice.

Diffraction patterns

The diffraction patterns for atoms through single-layer graphene for different kinetic energies are shown for He in Extended Data Fig. 2 and for H in Extended Data Fig 3.



Extended Data Figure 2 | Diffraction patterns for He passing through single-layer graphene corresponding to the profiles shown in Fig. 3(a) of the main text. Kinetic energy of the He atoms: (a) 459 eV, (b) 706 eV, (c) 958 eV, (d) 1208 eV. The black triangular shape is the shadow of the beam block on the detector.



Extended Data Figure 3 | Diffraction patterns for H passing through single-layer graphene corresponding to the profiles shown in Fig. 3(c) of the main text. Kinetic energy of the H atoms: (a) 963 eV, (b) 1162 eV, (c) 1262 eV, (d) 1581 eV. The black triangular shape is the shadow of the beam block on the detector.

Molecular dynamics simulation

To simulate kinetic and electronic energy transfer from a projectile to the graphene monolayer, we employed semi-classical Ehrenfest molecular dynamics (MD) within the framework of

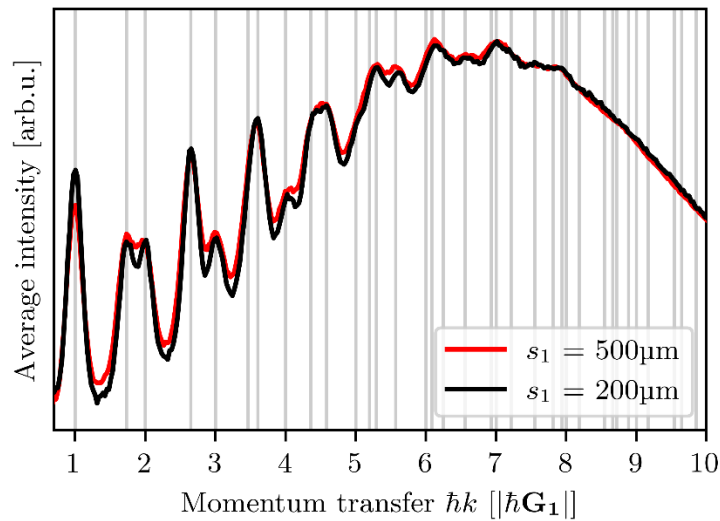
time-dependent density functional theory (TDDFT) using the GPAW code⁵⁴. This enables a combined treatment of classical nuclear degrees of freedom and quantum electronic degrees of freedom. Notably, Born-Oppenheimer MD would not result in any electronic energy transfer, but this can be adequately modelled using TDDFT⁴¹

Nuclear positions were propagated using the velocity-Verlet algorithm, while the electronic system evolution was handled by the semi-implicit Crank–Nicholson scheme with a timestep of 15 as. For a computationally efficient treatment of the required vacuum, we used localised atomic-orbital basis sets that were recently implemented for Ehrenfest MD⁵⁵. We use a double-zeta polarized (*dzp*) basis for graphene and He, and single-zeta (*sz*) for the H projectile, and a grid sampling of 0.2 Å with the PBE exchange-correlation functional⁵⁶.

Neutral H and He atoms were initially positioned sufficiently far (6 Å) above a 6×6 supercell of graphene. The projectile was then given a kinetic energy in the direction normal to the graphene plane towards the impact point, located at the centre of a graphene hexagon. The momentum transfer was determined by summing the momentum components in the lateral directions of the nearest carbon atoms adjacent to the impact site. The electronic energy transfer is inferred from the loss of the kinetic energy of the projectile⁴¹, see Fig. 1 of the main manuscript.

Angular resolution of the diffraction pattern

The traces depicted in Fig. 3(a) of the main manuscript have been recorded at an angular resolution of 1 mrad. As the spacing of the diffraction orders decreases with increasing beam energy E , also the effective angular resolution decreases with increasing E . To test whether this effect explains the observed loss of visibility for higher diffraction orders, we increased the angular resolution by a factor of 1.75 by decreasing the size of pinhole s_1 to 200 μm. This way we can compensate for the decrease in diffraction angle by a factor of 1.6 when increasing E from 460 to 1208 eV. As shown in Extended Data Fig. 4, the level of detail remains comparable, especially for higher diffraction angles. Thus, we conclude that the effect of collimation cannot account for the observed loss of visibility at larger diffraction angles.



Extended Data Figure 4 | Azimuthally averaged intensity for He at 1208 eV. Increasing the angular resolution from 1 mrad (red curve) to 0.6 mrad (black curve) has little effect on the pattern. In both cases, we observe no structured features for a scattering of more than 8 $|G_1|$.

References

- 41 Brand, C. *et al.* Coherent diffraction of hydrogen through the 246 pm lattice of graphene. *New J. Phys.* **21**, 033004 (2019).
- 50 Koopman, D. W. Measurement of charge-exchange cross sections for H^+ , H_2^+ , and He^+ ions. *Phys. Rev.* **154**, 79-85 (1967).
- 51 Hornberger, K., Gerlich, S., Haslinger, P., Nimmrichter, S. & Arndt, M. Colloquium: Quantum interference of clusters and molecules. *Rev. Mod. Phys.* **84**, 157-173 (2012).
- 52 Tripathi, M. *et al.* Cleaning graphene: Comparing heat treatments in air and in vacuum. *Phys. Status Solidi Rapid Res. Lett.* **11**, 1700124 (2017).
- 53 Trentino, A. *et al.* Atomic-Level Structural Engineering of Graphene on a Mesoscopic Scale. *Nano Lett.* **21**, 5179-5185 (2021).
- 54 Mortensen, J. J. *et al.* GPAW: An open Python package for electronic structure calculations. *J. Chem. Phys.* **160** (2024).
- 55 Zobač, V., Kuisma, M., Larsen, A. H., Rossi, T. & Susi, T. Ehrenfest dynamics with localized atomic-orbital basis sets within the projector augmented-wave method. Preprint at <https://arxiv.org/abs/2412.00168> (2024).
- 56 Perdew, J. P., Burke, K. & Ernzerhof, M. Generalized gradient approximation made simple. *Phys. Rev. Lett.* **77**, 3865-3868 (1996).

Acknowledgment

We thank Philippe Roncin and Alec Wodtke for useful discussions and Markus Arndt for comments on the manuscript. Funding by the Austrian Science Fund (FWF) [P 36264-N] is gratefully acknowledged by V.Z. and T.S.